Nuclear Science and Techniques (2026) 37:117
https://doi.org/10.1007/s41365-026-01947-w

Analysis of key factors on the neutron shielding performance for various boron-containing compounds

Zhi-Cheng Qian[1] · Zhi-Hong Zhang[1] · Jin-Sen Xie[2,3] · Jun Cai[1] · Jian-Hua Wang[1] · De-Feng Chen[1] · Chang-Yuan Li[1] · Xian-Wei Guo[1] · Hui-Quan Li[1]

Received: 5 March 2025 / Revised: 18 April 2025 / Accepted: 21 May 2025 / Published online: 10 April 2026

Abstract

Boron-containing compounds have gained significant attention as effective additives for enhancing the performance of composite materials. This study systematically investigates the key factors influencing the neutron shielding efficiency of various boron compounds, including mass density, boron content, and boron number density (atoms/nm^3), to establish guidelines for their optimal selection in radiation-shielding applications. The effective removal cross section (Σ_R) for fast neutrons was evaluated using Phy-X and NXcom software, whereas the macroscopic cross section (Σ) for thermal neutrons was calculated via Monte Carlo N-Particle (MCNP) simulations and manual computations. The results demonstrate that mass density and boron number density are the dominant factors for fast-neutron shielding, with Σ_R values ranging from 0.082 cm^{-1} (KBH_4) to 0.225 cm^{-1} (WB_2). For thermal neutrons, the boron number density is the primary determinant of shielding performance, with Σ values of 4070.34 cm^{-1} for GdB_6, 474.67 cm^{-1} for ZrB_{12}, and 447.37 cm^{-1} for B_4C. Notably, GdB_6 exhibits exceptional thermal neutron shielding owing to the high absorption cross section of ^{157}Gd. These findings provide critical insights for designing advanced shielding materials, emphasizing the synergistic effects of density and boron number density to optimize neutron attenuation.

Keywords Boron-containing compounds · Neutron shielding properties · Shielding impact factors

1 Introduction

The widespread application of nuclear technology and equipment has driven significant advancements in neutron shielding materials development. Among the various shielding elements, boron has emerged as a particularly effective component owing to its exceptionally high neutron absorption cross section [1–6] and cost-effectiveness. However, the practical implementation of boron for neutron shielding requires its incorporation into bulk materials, as elemental boron alone cannot meet the structural and functional requirements of shielding applications [7, 8]. To address this challenge, researchers have extensively investigated the integration of various boron compounds into different matrix materials. Commonly used boron compounds include boron carbide (B_4C), boron oxide (B_2O_3), titanium boride (TiB_2), tungsten diboride (W_2B_5/WB), boron nitride (BN), and boric acid (H_3BO_3). These compounds have been successfully incorporated into concrete matrices [9–11], composites [12–17], reactive sintered borides [18], glass systems [19, 20], and ceramics [21, 22]. These composite materials combine the neutron absorption capability of boron with the structural integrity and radiation stability of host materials. When boron forms compounds with transition metals or rare earth elements, the resulting materials exhibit enhanced macroscopic neutron capture cross sections and exceptional

This work was supported by the Key Laboratory of Advanced Nuclear Energy Design and Safety, Ministry of Education (No. KLANEDS202317).

✉ Zhi-Hong Zhang
zhangzhihong@sinap.ac.cn

✉ Jin-Sen Xie
jinsen_xie@usc.edu.cn

1 Shanghai Institute of Applied Physics, Chinese Academy of Sciences, Shanghai 201800, China

2 School of Nuclear Science and Technology, University of South China, Hengyang 421001, China

3 Key Lab of Advanced Nuclear Energy Design and Safety, Ministry of Education, Hengyang 421000, China

refractory properties [23]. This improvement is attributed to the synergistic effects between boron and metal atoms, which not only increase the neutron absorption efficiency but also enhance the thermal stability and mechanical strength.

Some boron metal compounds, especially metal borides such as borated steels (Fe_2B and FeB), hafnium diboride (HfB_2), and europium hexaboride (EuB_6), exhibit outstanding characteristics, including exceptional hardness and strength, high melting points, and robust chemical stability. These materials have been evaluated for use as neutron-absorbing pellets in control rods of nuclear reactors [24]. Numerous studies have focused on the processing, structure, and properties of boron compounds and boron-containing composites, driven by the demand for high-performance materials [25–28]. Serebrennikov et al. [29] demonstrated that MoB_2/B_4C multilayer systems outperform conventional materials (Mo, W, Pt) in terms of energy resolution and reflectivity, making them ideal for precision X-ray optics and synchrotron applications. Orlovskaya et al. [30] demonstrated that diboride ceramics, including zirconium diboride (ZrB_2), hafnium diboride (HfB_2), osmium diboride (OsB_2), and iridium diboride (IrB_2), exhibit exceptional mechanical properties, particularly in terms of hardness and Young's modulus.

Several studies have been conducted to quantitatively investigate the neutron shielding properties of boron compounds or boron-containing materials. Li et al. [31] investigated the shielding properties of composites made with boron ores from China for fast neutrons from a ^{252}Cf source. This study combined experimental measurements and Monte Carlo simulations to evaluate the total macroscopic removal cross sections, deposited energies, and absorbed doses. The results suggested that a higher boron content improved the neutron shielding capabilities of these materials. Korkut et al. conducted a comprehensive investigation into the fast-neutron shielding behavior (FNSB) of various boron compounds, including magnesium diboride (MgB_2), sodium borohydride ($NaBH_4$), and potassium borohydride (KBH_4) [32]. The results demonstrate that MgB_2 outperforms $NaBH_4$ and KBH_4 in terms of shielding efficiency, primarily because of its significantly higher boron content. In a follow-up study, Korkut et al. [33] investigated the effect of boron number density on neutron shielding in three boron ores by combining experiments with FLUKA simulations [34]. Their results confirmed that a higher boron density directly increases the Σ, thereby improving the shielding efficiency owing to enhanced neutron–boron interactions. Saryer et al. [35] studied neutron shielding in concrete composites with B_4C and FeB additives. Their results showed that both materials enhanced neutron attenuation; however, FeB outperformed B_4C owing to the combined benefits of boron neutron absorption and iron density, which improved energy dissipation. Ozdogan et al. [36] investigated the FNSB of composites containing B_4C, polyester resin, and titanium oxide in various proportions. The composites with higher boron contents exhibited larger Σ_R and Σ and lower neutron transmission ratios. Using experiments and simulations, Soltani et al. [37] studied the thermal neutron shielding behavior (TNSB) in B_4C-reinforced HDPE composites. They found that smaller boron particle sizes increased the neutron interaction probability, whereas higher boron content improved the shielding performance through enhanced neutron absorption.

In summary, incorporating an optimal amount of boron compounds into composite materials significantly enhances their neutron shielding capabilities. The choice of boron compounds for shielding applications is governed by two primary factors: neutron absorption efficiency and cost-processability balance. Compounds with a higher boron number density and boron content exhibit superior neutron shielding performance [31]. Although rare-earth borides such as GdB_6 show exceptional neutron shielding efficiency, their high cost is prohibitive; thus, some lightweight borides such as B_4C offer viable trade-offs between performance and affordability [24]. The effectiveness of these boron-based composites is primarily influenced by factors such as the boron content, boron number density, and particle size. These parameters collectively determine the ability of a material to attenuate neutrons, making them critical considerations in the design and optimization of advanced shielding solutions for applications in nuclear technology, medical radiation protection, and space exploration.

Owing to boron's high affinity for both light and heavy elements, it can form a wide range of compounds with different chemical compositions. It is important to systematically investigate the neutron shielding properties of boron compounds to screen suitable shielding materials. In this study, the thermal and fast-neutron shielding properties of various boron-containing compounds were analyzed. The key factors that may affect the including boron content (weight percent of boron), boron number density (number of boron atoms per unit), and mass density were studied. In Sect. 2, the theoretical basis is introduced; in Sect. 3, detailed information on the selected boron-containing compounds is introduced; and in Sect. 4, the neutron shielding performance of the boron-containing compounds is discussed.

2 Theoretical basis

2.1 Fast neutron effective removal cross section

Neutrons interact with matter via three primary mechanisms: elastic scattering, inelastic scattering, and neutron capture reactions. The likelihood of a fast or fission-energy neutron undergoing its first collision is quantified by the removal cross section [38]. This parameter represents the probability of removing neutrons from an uncollided beam, thereby reducing the flux of penetrating neutrons. The effective removal cross section remains relatively constant for neutron energies ranging from 2–12 MeV, making it a reliable metric for evaluating shielding materials within this energy range. For compounds or mixtures, the effective removal cross section can be calculated using the following equation:

$$\Sigma_R = \sum_i \rho_i (\Sigma_R/\rho)_i. \quad (1)$$

In this context, ρ_i represents the partial density of the i^{th} constituent element in the material. Here, ρ_i is defined as the density of the specific element, Σ_R/ρ_i denotes the mass removal cross section of the i^{th} element. These parameters are essential for calculating the overall removal cross section of the composite material, as they quantify the contribution of each element to the neutron shielding performance.

The partial density ρ_i can be calculated as the product of the weight fraction ω_i of the i^{th} element and the overall density of the sample, as expressed by the following equation:

$$\rho_i = \omega_i \times \rho_s. \quad (2)$$

In recent years, several user-friendly computational tools have been developed to facilitate the analysis and design of radiation-shielding materials. Notable examples include Phy-X [39], MERCSF-N [40], MRCsC [41], NXcom [42] and ParShied [43]. These programs leverage extensive databases of elemental removal cross sections and incorporate empirical models to predict the shielding performance of various materials. By providing accurate and efficient calculations, these tools have become indispensable for researchers and engineers in fields such as nuclear energy, medical physics, and space exploration. The integration of such software into the design process not only enhances the precision of the shielding material selection but also accelerates the development of innovative solutions tailored to specific radiation environments.

2.2 Thermal neutron transmission ratios and macroscopic cross section

The thermal neutron shielding properties of selected boron-based composite materials can be evaluated by analyzing their neutron transmission ratios and macroscopic cross sections (Σ). Although the Σ is expressed in units of cm^{-1}, which may cause confusion as it resembles a linear attenuation coefficient rather than the traditional cross section units of cm^2, it is widely used in the literature to describe neutron shielding performance. The value of Σ can be derived from neutron transmission measurements, providing a quantitative measure of a material's ability to attenuate thermal neutrons.

However, the experimental determination of these properties can be challenging, especially for boron-containing compounds such as TiB_2, MgB_2, and SiB_6, which typically exist as solid powders at room temperature. Handling powdered boron compounds under neutron irradiation necessitates specialized facilities and stringent safety protocols, which were inaccessible for this computational study. Several high-performance boron compounds (e.g., ZrB_{12} and GdB_6) are challenging to synthesize in the bulk quantities required for experimental neutron irradiation tests. To address these limitations, the Monte Carlo method has emerged as a powerful computational tool for simulating neutron interactions and predicting the shielding performance. For instance, Qian et al. [44] highlighted the effectiveness of Monte Carlo simulations in overcoming the experimental constraints.

In this study, the Monte Carlo N-Particle Transport Code, version 5 (MCNP5) [45] was employed to simulate the thermal neutron shielding behavior of boron composites. The simulation geometry, illustrated in Fig. 1, was carefully designed to replicate real-world conditions, ensuring accurate and reliable results. The use of MCNP5 circumvents the practical difficulties associated with handling powdered materials and provides a cost-effective and efficient alternative to experimental testing. By leveraging this computational approach, researchers can gain deeper insights into the shielding mechanisms of boron composites, optimize material compositions, and accelerate the development of advanced shielding solutions for applications in nuclear science and technology.

In the simulation setup, the thermal neutron source was positioned at the center of the shielding structure. The boron composite samples under investigation were modeled as spherical shells, with a neutron detector placed on the outer surface to measure the transmitted neutron flux. This detector utilizes the F2 tally function in MCNP5 to record neutron and secondary γ-ray flux data. To ensure the reliability of the simulation results, the MCNP5 code utilized the ENDF/B-VI neutron cross section database and set the total number of incident neutrons (nps) to 10^8 to reduce the statistical errors to less than 1%. During the simulation, the convergence of

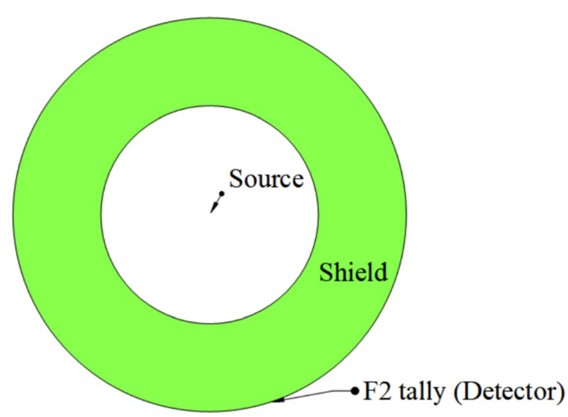

Fig. 1 (Color online) MCNP5 simulation geometry

the geometric model was verified by adjusting the spherical shell thickness (1–10 μm), and the results showed that the relative deviation of the Σ value due to thickness variation was less than 2%. More details of the MCNP5 input are presented in Table 1.

Based on the Beer–Lambert law [46], the macroscopic cross section (Σ) of a material can be determined using the following formula:

$$\Sigma(E) = -\frac{1}{x}\ln\left(\frac{I}{I_0}\right), \tag{3}$$

where I is the transmitted neutron flux, I_0 is the incident neutron flux, and x is the thickness of the shielding material. This relationship provides a direct method for calculating the macroscopic cross section, which quantifies the ability of a material to attenuate thermal neutrons. By combining this theoretical framework with MCNP5 simulation results, researchers can accurately assess the shielding performance of boron composites, even in scenarios where experimental measurements are impractical.

In addition, the macroscopic cross section (Σ) can be calculated manually using the following equation [47]:

$$\Sigma = \sum_i W_i(\Sigma_j/\rho)_i. \tag{4}$$

Here, W_i represents the partial density of the i^{th} constituent element, while $(\Sigma_j/\rho)_i$ is the neutron mass attenuation coefficient of the i^{th} constituent for a specific interaction type (j), as defined in Eq. (5).

$$\Sigma_j/\rho = \frac{N_{\text{A}}}{A}\cdot\sigma_{\text{t}} \tag{5}$$

Additionally, N_{A} stands for Avogadro's constant, A is the atomic weight of the i^{th} element, and σ_{t} is the microscopic cross section of the i^{th} element. These microscopic cross-section values can be retrieved from the comprehensive database available at the International Atomic Energy Agency (IAEA) website [48]. This resource provides essential nuclear data for accurate calculations and analyses in neutron shielding studies.

Table 1 The parameter details of MCNP5 input card

MCNP input	Parameter details
Thickness of shield	0.001 (cm)
SDEF	pos=0 0 0 par=1 erg= 2.53×10^{-8}
Detector	F2:n and F2:p
NPS	10^8

3 Materials and methods

In this study, a comprehensive series of boron-containing compounds with exceptional neutron absorption properties were systematically selected and investigated for their potential applications in nuclear shielding and radiation protection. The selected compounds, which exhibit a wide range of boron concentrations (ranging from 5.33% to 78.26%), mass densities (varying between 1.07 g/cm^3 and 14.15 g/cm^3), and boron number densities (spanning from 12.39 atoms/cm^3 to 118.03 atoms/nm^3), include both well-established and emerging materials: FeB, Fe_2B, KBH_4, $NaBH_4$, TiB_2, MgB_2, CaB_6, SiB_6, B_4C, ZrB_2, ZrB_{12}, Mo_2B, Mo_2B_5, WB_2, W_2B_5, NbB_2, CoB, NiB, CrB_2, TaB_2, VB_2, HfB_2, ReB_2, LuB_2, SmB_6, B_2O_3, and GdB_6. Furthermore, the TNSB of commercially available polyethylene–boron composites (BPE-5) [28] was evaluated alongside these boron compounds for comparative analysis. These materials were chosen based on their unique combination of neutron absorption capabilities, thermal stability, and mechanical properties, making them suitable for nuclear applications. The mass density values were obtained from reliable literature sources, including the comprehensive work by Knoch et al. on borides [24], recent studies by Orlovskaya et al. [30], and Serebrennikov et al. [29], as well as verified data from the reputable material database, MatWeb [49]. The comprehensive dataset, including detailed compositions, precise boron concentrations, and calculated boron number densities, is systematically presented in Table 2, providing a valuable reference for researchers in the field of nuclear materials science.

4 Results and discussion

4.1 Fast neutron shielding performance

The recently developed Phy-X software [39], which incorporates an updated database and a refined empirical model, was employed to calculate the macroscopic removal cross sections (Σ_{R}) for fast neutrons in various boron compounds. These results were compared with those obtained using the NXcom program [42], a well-established tool for radiation shielding analysis. The calculated Σ_{R} values for the investigated boron compounds are presented in Table 3. Notably, the results generated by the Phy-X software showed excellent agreement with those derived from the NXcom program, demonstrating the reliability and accuracy of both computational tools.

The influence of mass density on the fast-neutron shielding properties of various boron compounds is shown in Fig. 2. Among the studied materials, tungsten diboride

Table 2 The chemical compositions, density, boron concentration, and boron number density of the investigated samples

Composition	Density (g/cm^3)	Boron concentration (%)	Boron number density (atoms/nm^3)
FeB	7.00	16.22	63.22
Fe_2B	7.30	8.82	35.87
KBH_4	1.11	20.04	12.39
$NaBH_4$	1.07	28.58	17.03
TiB_2	4.38	31.11	75.89
MgB_2	2.57	47.07	67.37
CaB_6	2.43	61.81	83.64
SiB_6	2.43	69.78	94.43
B_4C	2.50	78.26	108.96
BN	3.49	43.55	84.58
ZrB_2	6.17	19.16	65.83
ZrB_{12}	3.61	58.71	118.03
Mo_2B	9.20	5.33	27.32
Mo_2B_5	7.20	21.97	88.11
WB_2	14.15	10.52	82.94
W_2B_5	11.00	12.82	78.52
NbB_2	6.80	18.88	71.49
CoB	7.25	15.50	62.58
NiB	7.13	15.55	61.76
CrB_2	5.22	29.37	85.37
TaB_2	11.2	10.68	66.59
HfB_2	10.5	10.80	63.17
ReB_2	12.7	10.40	73.58
LuB_2	9.76	11.00	59.77
SmB_6	5.07	30.19	85.23
B_2O_3	2.55	31.05	44.10
GdB_6	5.31	29.20	86.33
BPE-5	1.85	5	4.50

(WB_2) exhibits the highest values, attributed to its significantly higher mass density of 14.15 g/cm^3. In contrast, potassium borohydride (KBH_4), with the lowest mass density of 1.11 g/cm^3, demonstrates the lowest Σ_R values. This trend highlights a strong positive correlation between mass density and neutron shielding efficiency, as materials with greater densities tend to provide more effective neutron attenuation owing to increased atomic interactions. As shown in the figure, most of the data points align closely with the fitting curve, indicating a consistent relationship between the mass density and shielding performance. However, a few compounds, such as boron nitride (BN), iron boride (FeB), and potassium borohydride (KBH_4), deviated slightly from the curve. These deviations may arise from differences in the material composition, crystalline structure, or other factors influencing the neutron interaction probabilities. Despite these minor discrepancies, the overall trend confirms that boron compounds with higher mass densities generally exhibit superior fast-neutron shielding capabilities.

The relationship between the Σ_R values of boron compounds and their boron concentration, as well as boron number density, is illustrated in Figs. 3 and 4. As depicted in Fig. 3, tungsten diboride (WB_2) exhibits the highest Σ_R values despite having a relatively moderate boron concentration of 10.52%. This observation challenges the conventional assumption that materials with higher boron concentrations inherently possess superior neutron shielding properties. For instance, boron carbide (B_4C), which has the highest boron concentration at 78.26%, demonstrates only average fast-neutron shielding behavior compared to other boron compounds under study. This suggests that boron concentration alone is not the sole determinant of the shielding performance. Figure 3 further reveals that the FNSB of boron compounds does not exhibit a direct correlation with boron concentration. Instead, other factors, such as material density, atomic structure, and the presence of additional elements, may play significant roles in influencing the neutron attenuation efficiency. For example, the high density and unique atomic arrangement of WB_2 likely contribute to its exceptional shielding performance, even with a lower boron concentration. These findings underscore the complexity of neutron shielding mechanisms and highlight the need to consider multiple material properties when designing effective shielding solutions for neutron radiation.

Table 3 Effective removal cross section (cm^{-1}) calculated by Phy-X and NXcom program for different boron compounds

Composition	Phy-X	NXcom	Composition	Phy-X	NXcom	Composition	Phy-X	NXcom
FeB	0.191	0.191	BN	0.176	0.176	NiB	0.178	0.178
Fe_2B	0.179	0.179	ZrB_2	0.146	0.146	CrB_2	0.165	0.165
KBH_4	0.082	0.082	ZrB_{12}	0.145	0.145	TaB_2	0.180	0.180
$NaBH_4$	0.108	0.108	Mo_2B	0.160	0.160	HfB_2	0.170	0.170
TiB_2	0.140	0.140	Mo_2B_5	0.176	0.176	ReB_2	0.200	0.200
MgB_2	0.115	0.115	WB_2	0.225	0.225	LuB	0.159	0.159
CaB_6	0.109	0.109	W_2B_5	0.187	0.187	SmB6	0.131	0.131
SiB_6	0.119	0.119	NbB_2	0.158	0.158	B_2O_3	0.117	0.117
B_4C	0.140	0.140	CoB	0.183	0.183	GdB_6	0.134	0.134

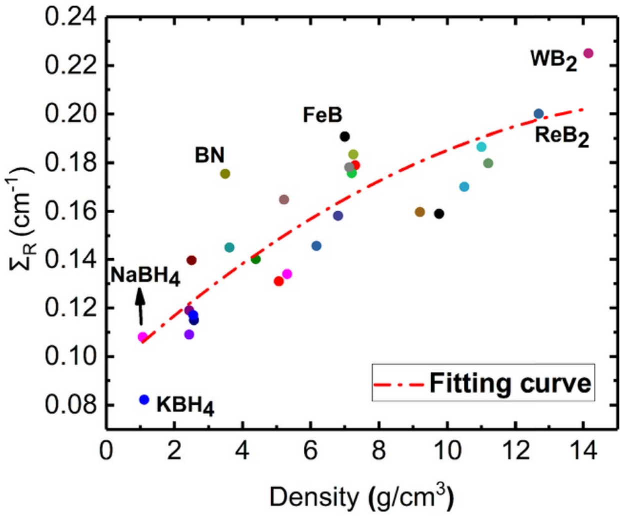

Fig. 2 (Color online) Effective removal cross section with mass density for different boron compounds

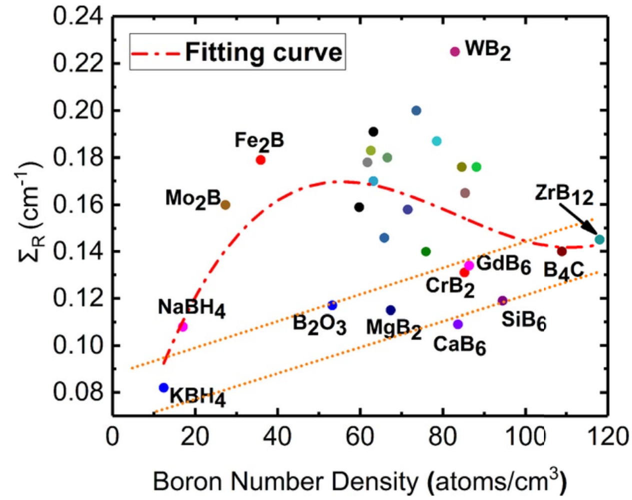

Fig. 4 (Color online) Effective removal cross section with boron number density for different the boron compounds

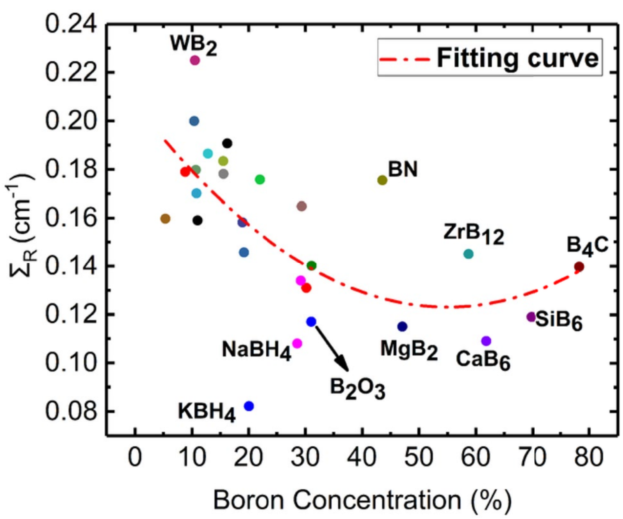

Fig. 3 (Color online) Effective removal cross section with boron concentration for different the boron compounds

The boron number density, which varies across boron compounds, is another critical factor that may influence the FNSB of these materials. Figure 4 illustrates the relationship between the values and the boron number density for various boron compounds. As shown in the figure, only a subset of compounds, including potassium borohydride (KBH_4), sodium borohydride ($NaBH_4$), boron trioxide (B_2 O), magnesium diboride (MgB_2), calcium hexaboride (CaB), silicon hexaboride (SiB_6), chromium diboride (CrB_2), gadolinium hexaboride (GdB_6), boron carbide (B_4C), and zirconium dodecaboride (ZrB_{12}), follow the expected trend where higher boron number density corresponds to larger Σ_R values. However, this trend did not hold for all compounds. For instance, tungsten diboride (WB_2) and calcium hexaboride (CaB_6) exhibit nearly identical boron number densities; however, their FNSB properties differ significantly. This discrepancy suggests that the boron number density alone cannot fully account for the variations in the neutron shielding performance. The non-proportional distribution of values with the number density of boron compounds may indicate that the number density is not the only key factor in the FNSB for boron compounds.

To determine whether the density and boron number density are the dominant factors influencing the FNSB of boron compounds, the variations in Σ_R values were analyzed as a function of the product of the density and boron number density, as illustrated in Fig. 5. An exponential fitting curve was also included to model this relationship. In contrast to the scattered distribution observed in Figs. 3 and 4, the data points in Fig. 5 exhibit a much closer alignment with the fitting curve, indicating a strong correlation. Only a few compounds, such as iron boride (Fe_2B), boron nitride (BN), and calcium hexaboride (CaB_6), deviated slightly from this trend. The exponential increase in Σ_R values with the product of the density and boron number density suggests that these two parameters collectively play a significant role in determining the FNSB of boron compounds. This relationship highlights the synergistic effect of density and boron number density on the neutron shielding performance, as higher values of both parameters enhance the probability of neutron interactions and energy absorption. The close fit of most data points to the exponential curve further supports the idea that these factors are the primary drivers of the shielding efficiency.

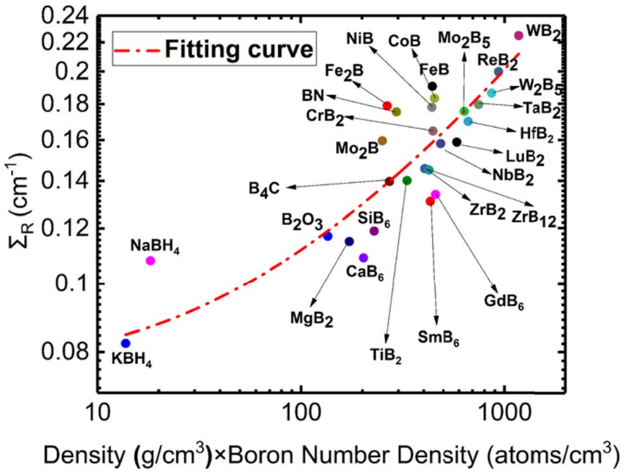

Fig. 5 (Color online) Effective removal cross section with the product of density and boron number density for different boron compounds

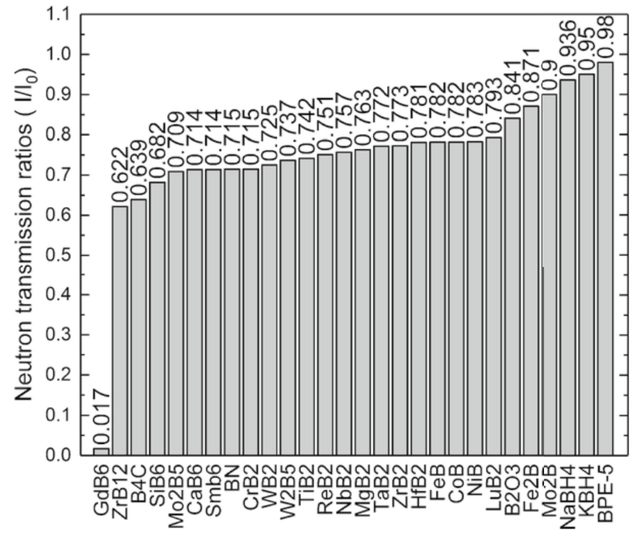

Fig. 6 Thermal neutron transmission ratios of boron compounds

Furthermore, the Σ_R values of commonly used neutron moderators demonstrate significant variation: water (H_2O) exhibits a Σ_R of 0.103 cm^{-1}, polyethylene ($(C_2H_4)_n$) shows 0.122 cm^{-1}, and graphite possesses 0.113 cm^{-1}. These materials have been extensively employed as fast-neutron moderators in radiation-shielding applications owing to their effective moderation properties. Notably, among boron-containing compounds, although potassium borohydride (KBH_4, Σ_R=0.082 cm^{-1}) and sodium borohydride ($NaBH_4$, Σ_R=0.108 cm^{-1}) exhibit slightly lower Σ_R values than water and graphite, the majority of boron compounds demonstrate superior Σ_R values. This enhanced performance highlights their exceptional fast-neutron shielding capabilities and suggests their promising potential for advanced radiation-shielding applications. Although this study shows that tungsten diboride (WB_2) exhibits the best performance in fast-neutron shielding (Σ_R=0.225 cm^{-1}), its high cost and complex manufacturing process limit its industrial application. In contrast, boron carbide (B_4C), with its lightweight properties (density of 2.50 g/cm^3) and high boron content (78.26%), has become the material of choice for reducing the weight and space of neutron shielding [3]. However, the low density of B_4C may lead to multiple scattering of fast neutrons, requiring the enhancement of the overall shielding efficiency through composite material design (e.g., mixing with high-density tungsten particles). Additionally, the brittleness of boron carbide may affect its stability under dynamic loading conditions, which could be improved in the future through nano-reinforcement or fiber composite technology.

4.2 Thermal neutron shielding performance

The thermal neutron transmission ratios (I/I_0) of various boron compounds are presented in Fig. 6. The results indicated that the transmission ratios of the selected boron composites ranged from 0.017 to 0.98. The lowest transmission ratio, observed for gadolinium hexaboride (GdB_6), signifies its exceptional TNSB.

The macroscopic cross section (Σ) values for the boron compounds studied at a neutron energy of 0.025 eV are presented in Table 4. Notably, the Σ values derived from the MCNP5 simulations show excellent agreement with those calculated manually using Eq. (4). To quantify the consistency between the simulated and calculated results, the percentage relative deviation (RD) was determined using Eq. (6) [50]. The RD values fell within a narrow range of 0.11–6.77%, demonstrating a high level of accuracy in the simulation outcomes. This close alignment between the simulated and manually calculated values underscores the reliability of the MCNP5 code in predicting neutron shielding properties and validates the robustness of the computational approach employed in this study. Furthermore, the secondary γ-ray fluences (cm^{-2}) are also presented in Table 4. As we known, ^{10}B can absorb the thermal neutrons and release secondary γ-rays, the reaction formula is given as Eq. (7).

$$RD = \left| \frac{\Sigma_{\mathrm{MCNP}} - \Sigma_{\mathrm{Calculation}}}{\Sigma_{\mathrm{MCNP}}} \right| \tag{6}$$

$$^{10}\mathrm{B} + \mathrm{n}(0.025\,\mathrm{eV}) \rightarrow {}^{4}\,\mathrm{He} + {}^{7}\,\mathrm{Li} + \gamma(0.48\,\mathrm{MeV}) \tag{7}$$

To gain deeper insights into the factors influencing the TNSB of the selected boron compounds, the Σ for thermal neutrons was analyzed in relation to the mass density, boron concentration, and boron number density, as illustrated in Figs. 7 and 8. These figures provide a comprehensive

Table 4 Σ values and secondary γ-rays fluence of boron compounds for thermal neutron

Composition	Σ (cm^{-1})		RD (%)	Secondary γ-rays fluence (cm^{-2})	Composition	Σ (cm^{-1})		RD (%)	Secondary γ-rays fluence (cm^{-2})
	MCNP	Manual calculated				MCNP	Manual calculated		
FeB	245.31	243.95	0.56	19,780.80	WB_2	321.74	319.19	0.80	24,987.80
FeB_2	138.33	138.96	0.45	11,837.90	W_2B_5	304.94	302.14	0.93	23,873.20
KBH_4	51.03	49.18	3.77	4603.91	NbB_2	278.37	275.07	1.20	22,024.30
$NaBH_4$	66.40	65.52	1.35	5933.93	CoB	245.28	243.28	0.82	20,071.40
TiB_2	298.46	292.20	2.14	23,398.80	NiB	244.89	239.22	2.37	20,239.10
MgB_2	269.86	259.11	4.15	21438.30	CrB_2	335.48	328.34	2.17	25,744.40
CaB_6	337.01	321.57	4.80	25,836.90	TaB_2	258.22	256.86	0.53	20,940.70
SiB_6	382.89	363.03	5.47	28,641.90	HfB_2	247.73	244.34	1.39	19,666.10
B_4C	447.37	418.99	6.77	32,357.80	ReB_2	286.45	285.02	0.50	22,343.60
BN	335.82	326.15	2.96	25,763.70	LuB_2	231.91	230.63	0.55	18,757.20
ZrB_2	257.02	253.42	1.42	20,572.40	SmB_6	336.39	329.39	2.13	26,119.60
ZrB_{12}	474.67	453.85	4.59	33,846.20	B_2O_3	173.03	169.78	1.91	14,486.60
Mo_2B	105.19	105.31	0.11	9148.80	GdB_6	4070.34	3985.34	2.13	150,413.00
Mo_2B_5	344.16	338.89	1.56	26,287.80	BPE-5	23.98	24.70	2.91	1948.53

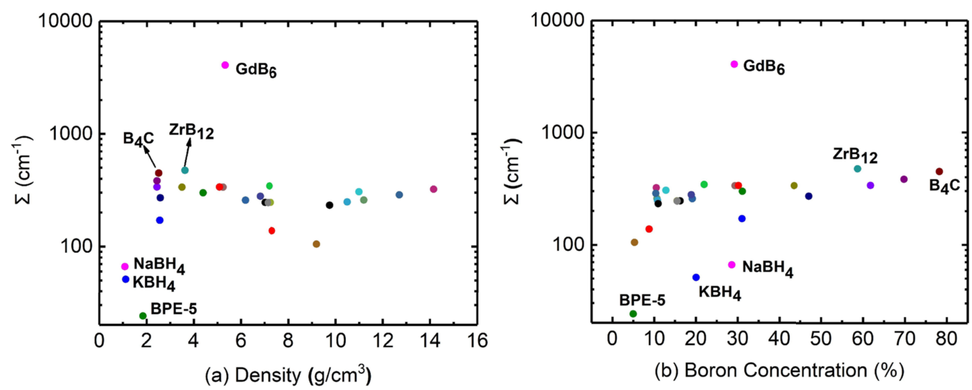

Fig. 7 (Color online) Macroscopic cross section of thermal neutrons with mass density and boron concentration for different the boron compounds

visualization of how these parameters collectively affect the shielding performance of boron-containing compounds. The distribution shown in Fig. 7a, b are similar, indicating that the Σ of thermal neutrons is not proportional to density and boron concentration.

As shown in Fig. 8, most data points closely align with the fitting curve, except for gadolinium hexaboride (GdB_6). This trend indicates that boron compounds with higher boron number densities generally exhibit larger Σ values, reflecting their enhanced thermal neutron shielding capabilities. Notably, GdB_6 exhibits a significantly higher Σ value than other boron compounds, attributable to the extraordinarily high thermal neutron cross section of ^{157}Gd (253909.786 cm^{-1}) at 0.025 eV, which far exceeds that of ^{10}B (3844.16 cm^{-1}), far exceeding the Σ value of ^{10}B. Owing to its relatively low boron number density, the TNSB of commercially available polyethylene–boron composites (BPE-5) demonstrates inferior performance

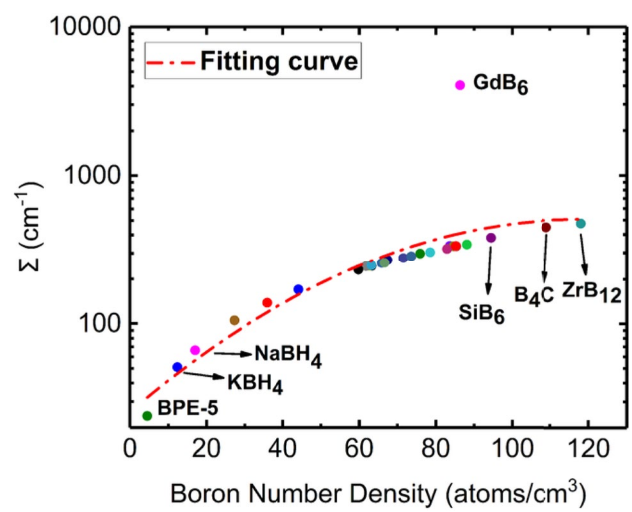

Fig. 8 (Color online) Macroscopic cross section of thermal neutrons with boron number density for different the boron compounds

compared to other boron compounds. In addition to GdB_6, B_4C (Σ=447.37 cm^{-1}) and ZrB_{12} (Σ=474.67 cm^{-1}) also demonstrate outstanding TNSB.

Among the various factors examined, the boron number density emerged as the most significant determinant of TNSB in boron compounds. However, further research is essential to fully understand the generation of secondary particles resulting from neutron capture in these materials. As is widely recognized, neutron capture reactions, such as the (n, α) reaction in ^{10}B and similar reactions in elements such as ^{149}Sm and ^{157}Gd, produce secondary gamma rays [51]. The energy of the secondary gamma rays produced by ^{10}B, ^{149}Sm, and ^{157}Gd was 0.48 MeV, 7.89 MeV, and 7.88 MeV, respectively. Furthermore, as TNSB increased, a corresponding increase in secondary gamma-ray production was observed, as shown in Table 4. These secondary emissions must be carefully considered in the design of radiation-shielding systems, as they can compromise the overall shielding effectiveness. To address this, the design of multilayer shielding structures combining an outer layer of high-density materials (e.g., tungsten or lead) with an inner layer of high boron number density materials (e.g., B_4C or GdB_6) could optimize the overall performance by simultaneously attenuating neutrons and minimizing secondary radiation [16, 52–56]. This approach not only improves neutron attenuation but also reduces the secondary radiation burden, making boron-based materials more versatile and effective for radiation-shielding applications. Continued exploration of these compositional adjustments is vital for advancing the development of next-generation shielding materials that meet the stringent demands of modern radiation protection.

4.3 Future research directions

This study primarily focused on the influence of the boron number density, mass density, and boron content on the neutron shielding performance. However, it is important to acknowledge that the structural morphology, such as porosity, grain boundaries, and nanoscale material design, can also play a significant role in neutron attenuation. These microstructural characteristics may affect the real-world performance of shielding materials by altering the neutron interaction probabilities, scattering mechanisms, and overall material integrity. To address these gaps, further investigations are recommended in the following areas: (1) microstructural optimization: systematic studies on how porosity, grain size, and phase distribution influence neutron shielding in boron composites [57, 58]. (2) Advanced fabrication techniques: methods such as spark plasma sintering or additive manufacturing to control the morphology and minimize defects [59, 60].

WB_2 is a refractory ceramic characterized by exceptional hardness (~ 20 GPa) and high thermal stability (melting point ~ 2800 °C) [24], making it ideal for use in extreme environments. Its dense atomic structure and tungsten content enhance radiation-shielding performance; however, its high brittleness and poor processability necessitate composite designs (e.g., metal matrix bonding) for practical applications [16]. GdB_6 offers outstanding neutron absorption owing to gadolinium's high cross section, coupled with moderate mechanical strength (~ 15 GPa) and thermal stability (melting point ~ 2500 °C) [51, 52]; however, its mechanical properties often require reinforcement (e.g., polyethylene matrix integration). ZrB_{12} stands out for its exceptional thermal resilience (melting point > 3000 °C) and high boron number density (118.03 atoms/nm^3), providing an optimal balance of neutron attenuation and structural integrity for high-temperature nuclear components [23, 61]. Future efforts should focus on optimizing the material composition and structural design to balance the shielding efficiency, cost, and processability, thereby promoting the practical application of boron-based composite materials in the nuclear energy, aerospace, and medical fields.

Fabrication techniques play a pivotal role in optimizing the neutron shielding performance of boron-containing composites and alloys. Advanced methods such as spark plasma sintering and powder metallurgy have been employed to fabricate dense, homogeneous composites such as B_4C/Al and WB/Al, ensuring uniform boron dispersion and enhanced mechanical integrity [62]. For polymer-based shields (e.g., HDPE/B_4C), melt blending and hot pressing are widely used to achieve optimal particle–matrix adhesion, whereas cold spraying has emerged for creating layered structures with minimal porosity [63]. In alloy systems (e.g., borated steels), arc melting and mechanical alloying are critical for achieving high boron solubility and structural stability under irradiation [24]. Future efforts should focus on scalable techniques, such as additive manufacturing, to address challenges in complex geometries and industrial adoption.

Future research could also explore the development of multi-component boron-based composite materials, such as combining GdB_6 with polyethylene, to leverage the synergistic effects of hydrogen moderation and boron capture for enhanced shielding efficiency. The synergistic use of ZrB_{12} and GdB_6 in nuclear reactor control rods is worth exploring. The high-temperature stability of ZrB_{12} and its high boron number density render it suitable for fast-neutron absorption, whereas GdB_6 can efficiently capture thermal neutrons. Such combinations can optimize the neutron absorption dynamics of control rods while enhancing their durability in extreme environments.

5 Summary

In this study, the fast-neutron shielding properties of selected boron compounds were evaluated using the Phy-X and NXcom programs to analyze their Σ_R. The analysis of Σ_R in relation to mass density, boron content, boron number density, and the product of mass density and boron number density revealed that mass density and boron number density are the primary factors influencing fast-neutron shielding performance. Specifically, the Σ_R values of boron compounds ranged from 0.082 cm^{-1} (KBH_4) to 0.225 cm^{-1} (WB_2), with mass density and boron number density identified as dominant factors. An exponential correlation was observed between Σ_R and the product of these two parameters, with WB_2 (ρ=14.15 g/cm^3, boron number density of 82.94 atoms/nm^3) exhibiting the highest Σ_R.

To assess the thermal neutron shielding behavior, the Σ values were determined using both the MCNP5 simulation code and manual calculations. The results from these two methods show excellent agreement, with Σ varying from 23.98 cm^{-1} (BPE-5) to 4070.34 cm^{-1} (GdB_6). GdB_6 achieving exceptional performance owing to the high absorption cross section of ^{157}Gd. In addition, the key factors affecting thermal neutron shielding, such as mass density, boron content, and boron number density, were systematically evaluated. The findings indicate that a higher boron number density correlates with superior Σ values, highlighting its critical role in enhancing thermal neutron attenuation. The results also revealed that boron compounds with higher boron number densities, such as B_4C (Σ=447.37 cm^{-1}) and ZrB_{12} (Σ=474.67 cm^{-1}), demonstrated outstanding thermal neutron shielding performances, making them promising candidates for use as additives in the development of advanced radiation-shielding materials.

Although Monte Carlo simulations provide a robust theoretical framework for evaluating neutron shielding properties, this study acknowledges the absence of experimental validation. To mitigate these limitations, the MCNP5 results were cross-validated with manual calculations, achieving excellent agreement. Therefore, future studies should prioritize experimental validation to improve accuracy, particularly for industrial-grade shielding composites.

In conclusion, this study systematically reveals the key factors affecting the neutron shielding performance of boron compounds and provides theoretical support for the engineering applications of materials such as WB_2, GdB_6, B_4C, and ZrB_{12}. These findings can provide valuable guidance for future researchers in designing next-generation neutron shielding materials, such as composites, glasses, and ceramics. Future efforts should focus on optimizing the generation of secondary particles resulting from neutron capture in these materials and optimizing the elemental composition to minimize secondary gamma radiation. By addressing these challenges, boron-based materials can be further developed to meet the stringent demands of modern radiation protection, paving the way for the next generation of advanced shielding solutions.

Author contributions Zhi-Cheng Qian was responsible for the writing, editing, and revising of the manuscript. Jun Cai and Jin-Sen Xie contributed to the critical review and revision of the paper. Chang-Yuan Li and Jian-Hua Wang conducted the methodology design and investigation. Hui-Quan Li and De-Feng Chen performed data validation and analysis. Zhi-Hong Zhang and Xian-Wei Guo handled the software development and computational work.

Data availability The data that support the findings of this study are openly available in Science Data Bank at https://cstr.cn/31253.11.sciencedb.j00186.00984 and https://doi.org/10.57760/sciencedb.j00186.00984.

Declarations

Conflict of interest The authors declare that they have no conflict of interest.

References

1. S.Y. Rasul, B. Aktas, D. Yilmaz et al., Impact of HfO_2 on the structural, thermal, gamma, and neutron shielding properties of boro-tellurite glasses. Mater. Chem. Phys. **174**, 113993 (2025). https://doi.org/10.1016/j.inoche.2025.113993
2. B.B. Solak, B. Aktas, D. Yilmaz et al., Exploring the radiation shielding properties of B_2O_3-PbO-TeO_2-CeO_2-WO_3 glasses: A comprehensive study on structural, mechanical, gamma, and neutron attenuation characteristics. J. Alloys Compd. **312**, 128672 (2024). https://doi.org/10.1016/j.matchemphys.2023.128672
3. K. Dogru, B. Aktas, A. Acikgoz et al., Structural, thermal, and radiation shielding properties of B_2O_3-TeO_2-Bi_2O_3-CdO-Tm_2O_3 glasses: The role of Tm_2O_3. Ceram. Int. **50**, 47384–47394 (2024). https://doi.org/10.1016/j.ceramint.2024.09.088
4. B. Aktas, A. Acikgoz, D. Yilmaz et al., The role of TeO_2 insertion on the radiation shielding, structural and physical properties of borosilicate glasses. J. Nucl. Mater. **563**, 153619 (2022). https://doi.org/10.1016/j.jnucmat.2022.153619
5. B. Aktas, S. Yalcin, K. Dogru et al., Structural and radiation shielding properties of chromium oxide doped borosilicate glass. Radiat. Phys. Chem. **156**, 144–149 (2019). https://doi.org/10.1016/j.radphyschem.2018.11.012
6. D. Yılmaz, B. Aktaş, Ş. Yalçın et al., Erbium oxide and Cerium oxide-doped borosilicate glasses as radiation shielding material. Radiat. Eff. Defects Solids **175**, 458–471 (2020). https://doi.org/10.1080/10420150.2019.1674301
7. M.G. Dong, X.X. Xue, V.P. Singh et al., Shielding effectiveness of boron-containing ores in Liaoning province of China against gamma rays and thermal neutrons. Nucl. Sci. Tech. **29**, 58 (2018). https://doi.org/10.1007/s41365-018-0397-x
8. M.G. Dong, X.X. Xue, Y. Elmahroug et al., Investigation of shielding parameters of some boron containing resources for gamma ray and fast neutron. Results Phys. **13**, 102129 (2019). https://doi.org/10.1016/j.rinp.2019.02.065

9. E. Zorla, C. Ipbüker, A. Biland et al., Radiation shielding properties of high performance concrete reinforced with basalt fibers infused with natural and enriched boron. Nucl. Eng. Des. **313**, 306–318 (2017). https://doi.org/10.1016/j.nucengdes.2016.12.029
10. H.L. Zhang, X.B. Zuo, Q.Q. Sun et al., Preparation of h-BN@ZnO composite epoxy coating for improve durability and antibacterial properties of concrete. Constr. Build. Mater. **438**, 137082 (2024). https://doi.org/10.1016/j.conbuildmat.2024.137082
11. J. Li, S.D. Liu, P.W. Sun et al., Study on shielding properties of concretes with boron-containing blast furnace slag as aggregate for portable D–D neutron sources. Constr. Build. Mater. **460**, 139841 (2025). https://doi.org/10.1016/j.conbuildmat.2024.139841
12. H. Chen, W. Wang, Y. Li et al., The design, microstructure and tensile properties of B_4C particulate reinforced 6061Al neutron absorber. composites. J. Alloys Compd. **632**, 23–29 (2015). https://doi.org/10.1016/j.jallcom.2015.01.048
13. H. Chen, H. Nie, W. Wang et al., A novel neutron shielding AA6061/B_4C laminar composite fabricated by powder metallurgy: SPS-HER. J. Alloys Compd. **806**, 1445–1452 (2019). https://doi.org/10.1016/j.jallcom.2019.07.133
14. M.Q. Gao, H.J. Kang, Z.N. Chen et al., Effect of reinforcement content and aging treatment on microstructure and mechanical behavior of B_4C_p/6061Al composites. Mater. Sci. Eng., A **744**, 682–690 (2019). https://doi.org/10.1016/j.msea.2018.12.042
15. J. Wang, D.L. Ren, L.L. Chen et al., Initial investigation of B_4C-TiB_2 composites as neutron absorption material for nuclear reactors. J. Nucl. Mater. **539**, 152275 (2020). https://doi.org/10.1016/j.jnucmat.2020.152275
16. J. Qiao, Q. Zhang, Y.C. Zhou et al., Microstructure and properties of WB/Al nuclear shielding composites prepared by spark plasma sintering. Ceram. Int. **48**, 31952–31964 (2022). https://doi.org/10.1016/j.ceramint.2022.07.131
17. Z.P. Huo, Y.D. Lu, H. Zhang et al., Sm_2O_3 micron plates/B_4C/HDPE composites containing high specific surface area fillers for neutron and gamma-ray complex radiation shielding. Compos. Sci. Technol. **251**, 110567 (2024). https://doi.org/10.1016/j.compscitech.2024.110567
18. J.M. Marshall, D. Walker, P.A. Thomas, HRXRD study of the theoretical densities of novel reactive sintered boride candidate neutron shielding materials. Nucl. Mater. Energy **22**, 100732 (2020). https://doi.org/10.1016/j.nme.2020.100732
19. X. Du, T.T. Wang, B.H. Duan et al., Effects of energy deposition on mechanical properties of sodium borosilicate glass irradiated by three heavy ions: P, Kr, and Xe. Nucl. Sci. Tech. **30**, 115 (2019). https://doi.org/10.1007/s41365-019-0632-0
20. Y. Cao, T. Ou, H. Xue et al., Effect of boron doping on the irradiation resistance of iron phosphate glass: insights from mechanical properties and chemical stability. J. Non-Cryst. Solids **646**, 123238 (2024). https://doi.org/10.1016/j.jnoncrysol.2024.123238
21. M.Y. Yang, Q.C. Jia, C. Chen et al., Crystallization of low-k boron calcium silicate glass-ceramics induced by β-$CaSiO_3$ seed crystals. Ceram. Int. **51**, 14736–14745 (2025). https://doi.org/10.1016/j.ceramint.2025.01.315
22. T. Li, S. Gu, Z. Xu et al., Effect of hexagonal boron nitride content on the anisotropy of hot-press-sintered AlN/BN composite ceramics. Ceram. Int. **50**, 29486–29493 (2024). https://doi.org/10.1016/j.ceramint.2024.05.243
23. M.N. Mohammad, The behavior of HfB_2 under neutron irradiation. Nucl. Sci. Tech. **27**, 27 (2016). https://doi.org/10.1007/s41365-016-0032-7
24. H. Knoch, Borides. Concise Encyclopedia of Advanced Ceramic Materials 35–38 (1991). https://doi.org/10.1016/B978-0-08-034720-2.50020-4
25. R. Borthakur, V. Chandrasekhar, Boron-heteroelement (B-E; E = Al, C, Si, Ge, N, P, As, Bi, O, S, Se, Te) multiply bonded compounds: recent advances. Coord. Chem. Rev. **429**, 213647 (2021). https://doi.org/10.1016/j.ccr.2020.213647
26. T. Dewen, Z. Shuliang, Y. Liang, Influence of boron contents on microstructure, mechanical properties and shielding effect of Fe–W–C alloy. J. Alloys Compd. **803**, 466–475 (2019). https://doi.org/10.1016/j.jallcom.2019.06.061
27. C. Zhu, G. Li, J. Wang et al., Performance improvement in neutron-shielding ultra-high performance mortar prepared with alkaline-treated boron carbide. J. Build. Eng. **71**, 106435 (2023). https://doi.org/10.1016/j.jobe.2023.106435
28. G. Almisned, G. Susoy, H.O. Tekin et al., Neutron transmission analysis in borated polyethylene, boron carbide, and polyethylene: insights from MCNP6 simulations. Radiat. Phys. Chem. **218**, 111585 (2024). https://doi.org/10.1016/j.radphyschem.2024.111585
29. D.A. Serebrennikov, O.A. Dikaya, K.Y. Maksimova et al., Multilayers made of boron-based compounds: simulation of optical properties and prospects for X-ray applications. Results Phys. **15**, 102804 (2019). https://doi.org/10.1016/j.rinp.2019.102804
30. N. Orlovskaya, H. Hyer, Y. Sohn et al., ZrB_2, HfB_2, OsB_2 and IrB_2 boride ceramics: processing, structure, and properties. In Encyclopedia of materials: technical ceramics and glasses. **2**, 200–215 (2021). https://doi.org/10.1016/B978-0-12-818542-1.00055-2
31. Z. Li, X. Xue, S. Liu et al., Effects of boron number per unit volume on the shielding properties of composites made with boron ores from China. Nucl. Sci. Tech. **23**, 344–348 (2012). https://doi.org/10.13538/j.1001-8042/nst.23.344-348
32. T. Korkut, A. Karabulut, G. Budak et al., Investigation of fast neutron shielding characteristics depending on boron percentages of MgB_2, $NaBH_4$ and KBH_4. J. Radioanal. Nucl. Chem. **286**, 61–65 (2010). https://doi.org/10.1007/s10967-010-0619-0
33. T. Korkut, A. Karabulut, G. Budak et al., Investigation of neutron shielding properties depending on number of boron atoms for colemanite, ulexite and tincal ores by experiments and FLUKA Monte Carlo simulations. Appl. Radiat. Isot. **70**, 341–345 (2012). https://doi.org/10.1016/j.apradiso.2011.09.006
34. A. Ferrari, P. Sala, A. Fasso et al., FLUKA: a multi-particle transport code. CERN-2005-10 INFN/TC 05/11, SLAC-R-773 (2005)
35. D. Saryer, R. Küçer, N. Küçer, Neutron shielding properties of concretes containing Boron Carbide and Ferro–Boron. World Conf. Technol. Innov. Entrep. **195**, 1752–1756 (2015). https://doi.org/10.1016/j.sbspro.2015.06.320
36. H. Ozdogan, M.R. Kacal, O. Kilicoglu et al., Experimental, simulation, and theoretical investigations of gamma and neutron shielding characteristics for reinforced with boron carbide and titanium oxide composites. Radiat. Phys. Chem. **226**, 112167 (2025). https://doi.org/10.1016/j.radphyschem.2024.112167
37. Z. Soltani, A. Beigzadeh, F. Ziaie et al., Effect of particle size and percentages of Boron carbide on the thermal neutron radiation shielding properties of HDPE/B_4C composite: Experimental and simulation studies. Radiat. Phys. Chem. **127**, 182–187 (2016). https://doi.org/10.1016/j.radphyschem.2016.06.027
38. F.C. Hila, J.F.M. Jecong, C.A.M. Dingle et al., Generation of fast neutron removal cross sections using a multi-layered spherical shell model. Radiat. Phys. Chem. **189**, 109735 (2021). https://doi.org/10.1016/j.radphyschem.2021.109735
39. E. Şakar, ö. F. Özpolat, B. Aılım et al., Phy-X / PSD: development of a user friendly online software for calculation of parameters relevant to radiation shielding and dosimetry. Radiat. Phys. Chem. **166**, 108496 (2020). https://doi.org/10.1016/j.radphyschem.2019.108496
40. A.M. El-Khayatt, A. El-Sayed Abdo, MERCSF-N: A program for the calculation of fast neutron removal cross sections in composite

shields. Ann. Nucl. Energy **36**, 832–836 (2009). https://doi.org/10.1016/j.anucene.2009.01.013
41. M.G. El-Samrah, A.M. El-Mohandes, A.M. El-Khayatt et al., MRCsC: a user-friendly software for predicting shielding effectiveness against fast neutrons. Radiat. Phys. Chem. **182**, 109356 (2021). https://doi.org/10.1016/j.radphyschem.2021.109356
42. A.M. El-Khayatt, NXcom: a program for calculating attenuation coefficients of fast neutrons and gamma-rays. Ann. Nucl. Energy **38**, 128–132 (2011). https://doi.org/10.1016/j.anucene.2010.08.003
43. Y. Elmahroug, ParShield: a computer program for calculating attenuation parameters of the gamma rays and the fast neutrons. Ann. Nucl. Energy **76**, 94–99 (2015). https://doi.org/10.1016/j.anucene.2014.09.044
44. Z.C. Qian, J. Cai, C.Y. Li et al., Influence of PbO content on the gamma ray shielding properties of lead boro-telluro-phosphate glasses. Radiat. Phys. Chem. **185**, 109516 (2021). https://doi.org/10.1016/j.radphyschem.2021.109516
45. Monte Carlo Team, MCNP - Version 5, vol. I. Overview and Theory, LA-UR-031987 (2003)
46. G. Su, F. Deng, C. Sun et al., A study on hybrid light extinction model and inversion based on Lambert-Beer Law. Opt. Commun. **577**, 131342 (2025). https://doi.org/10.1016/j.optcom.2024.131342
47. Z.F. Li, X.X. Xue, P.N. Duan et al., Preparation and thermal/fast neutron shielding properties of novel boron containing ore composites. MSF **743–744**, 613 (2013). https://doi.org/10.4028/www.scientific.net/msf.743-744.613
48. IAEA. https://www-nds.iaea.org/
49. MatWeb. https://www.matweb.com/
50. A. Sharma, Simulation of shielding parameters for TeO_2-WO_3-GeO_2 glasses using FLUKA code. Results Phys. **13**, 102199 (2019). https://doi.org/10.1016/j.rinp.2019.102199
51. D. Castley, C. Goodwin, J. Liu, Computational and experimental comparison of boron carbide, gadolinium oxide, samarium oxide, and graphene platelets as additives for a neutron shield. Radiat. Phys. Chem. **165**, 108435 (2019). https://doi.org/10.1016/j.radphyschem.2019.108435
52. X.Y. Wang, J.Y. Chen, Q. Zhang et al., Boron shielding design for neutron and gamma detectors of a pulsed neutron tool. Nucl. Sci. Tech. **36**, 16 (2025). https://doi.org/10.1007/s41365-024-01605-z
53. G. Hu, H. Hu, Q. Yang et al., Study on the design and experimental verification of multilayer radiation shield against mixed neutrons and γ-rays. Nucl. Eng. Technol. **52**, 178–184 (2020). https://doi.org/10.1016/j.net.2019.07.016
54. C.L. Sheng, M.A. Sazali, A.A. Abu Bakar et al., Polyethylene composite doped with cadmium and tungsten oxide for neutron-gamma multilayer shielding. Radiat. Phys. Chem. **229**, 112506 (2025). https://doi.org/10.1016/j.radphyschem.2024.112506
55. J. Qiao, L. Xu, Y. Wang et al., Fabrication and properties of (W+B)/Al hybrid composites for nuclear radiation shielding. J. Alloys Compd. **969**, 172292 (2023). https://doi.org/10.1016/j.jallcom.2023.172292
56. M. Salimi, N. Ghal-Eh, E.A Amirabadi, Characterization of a new shielding rubber for use in neutron–gamma mixed fields. Nucl. Sci. Tech. **29**, 36 (2018). https://doi.org/10.1007/s41365-018-0371-7
57. S.G. Jeong, S.Y. Ahn, E.S. Kim et al., Effect of substrate yield strength and grain size on the residual stress of direct energy deposition additive manufacturing measured by neutron diffraction. Mater. Sci. Eng., A **851**, 143632 (2022). https://doi.org/10.1016/j.msea.2022.143632
58. A.D. Hua, Y.S. Su, Y.P. Cai et al., Strengthened high-temperature resistance in B_4C/SiC/2024Al composite via SiC nanowires pinning grain boundary. J. Alloys Compd. **1000**, 175046 (2024). https://doi.org/10.1016/j.jallcom.2024.175046
59. J. Wang, D.L. Ren, L.L. Chen et al., Initial investigation of B_4C-TiB_2 composites as neutron absorption material for nuclear reactors. J. Nucl. Mater. **539**, 152275 (2020). https://doi.org/10.1016/j.jnucmat.2020.152275
60. Y.K. Kim, S.Y. Kim et al., Microfluidic exploitation of liquid crystal properties of boron nitride nanotubes and enhancing neutron shielding with aligned structure. Small Struct. **5**, 2400281 (2024). https://doi.org/10.1002/sstr.202400281
61. X.H. Li, Y.L. Yong, H.L. Cui et al., Mechanical behavior, electronic and phonon properties of ZrB_{12} under pressure. J. Phys. Chem. Solids **117**, 173–179 (2018). https://doi.org/10.1016/j.jpcs.2018.02.033
62. C. Kursun, Y. Gaylan, A.O. Yalcin et al., Advanced neutron and γ-ray shielding characteristics of nanostructured (90–x)Al-xGd_2O_3 composites reinforced by tungsten. J. Alloys Compd. **1010**, 177372 (2025). https://doi.org/10.1016/j.jallcom.2024.177372
63. C. Kursun, M. Gao, S. Guclu et al., Measurement on the neutron and gamma radiation shielding performance of boron-doped titanium alloy $Ti_{50}Cu_{30}Zr_{15}B_5$ via arc melting technique. Heliyon **9**, 21696 (2023). https://doi.org/10.1016/j.heliyon.2023.e21696